Research Square

Preprints are preliminary reports that have not undergone peer review.
They should not be considered conclusive, used to inform clinical practice,
or referenced by the media as validated information.

Prussian blue nanozyme-based colorimetric biosensor for rapid visual quantification of β-galactosidase-positive foodborne bacteria in bottled water and milk

Shangqing Li
Minnan Normal University
Lingling Su
Minnan Normal University
Jiayi Luo
Minnan Normal University
Shunxing Li
lishunxing@mnnu.edu.cn
Minnan Normal University
Zhaojing Huang
Minnan Normal University
Fengying Zheng
Minnan Normal University
Fengjiao Liu
Minnan Normal University
Luxiu Lin
Minnan Normal University
Jie Chen
Minnan Normal University

Research Article

Keywords: Bacterial Detection, Peroxidase, Colorimetric Sensing, Proportional Fluorescence Sensing

Posted Date: November 24th, 2026

DOI: https://doi.org/10.21203/rs.3.rs-11441020/v1

License: This work is licensed under a Creative Commons Attribution 4.0 International License.
Read Full License

Additional Declarations: No competing interests reported.

Abstract

Infections caused by foodborne pathogens pose a serious challenge to global public health. Conventional detection approaches suffer from inherent drawbacks, e.g., time-consuming, operationally complex, high-cost, and instrument-dependent. Thus, to develop a rapid, sensitive, convenient, and cost-effective novel visual sensor for bacterial detection remains an urgent need. Herein, we rationally designed a novel sensing strategy based on β-galactosidase-positive bacteria (β-gal) can interact with a peroxidase-like nanomaterials, i.e., Prussian blue nanoparticles (PB NPs). The PB NPs-based β-galactosidase detection approach enables highly specific recognition toward β-galactosidase-positive bacteria with the linear range from 8×10^1 to 8×10^7 CFU/mL ($R^2 = 0.9984$). Generally, PB NPs firstly catalyze H_2O_2-mediated oxidation of colorless 3,3',5,5'-tetramethylbenzidine (TMB) and yield a blue signal (oxidized TMB, ox-TMB). Upon the trigger of target bacteria, p-aminophenyl-β-D-galactopyranoside (PAPG) is subsequently hydrolyzed into reductive p-aminophenol (PAP), which suppresses ox-TMB, i.e., the blue signal is negatively correlated with the bacterial concentration. The turnaround time from sample generation to measurement has been reduced by half. The novel approach achieves real-time and sensitive detection for β-galactosidase-positive bacteria flora, showing excellent feasibility, robustness, and great potential for practical applications.

Introduction

Food-borne pathogen are a primary source of human illness, capable of causing acute poisoning symptoms and even life-threatening conditions[1, 2]. β-galactosidase-positive bacteria, defined by their production of β-galactosidase, are ubiquitous in spoiled food and encompass hundreds of species across at least six phyla. *E. coliserves* (*E. coli*) is selected as an ideal model for β-galactosidase verifying assay sensitivity and detection kinetics due to its robust β-galactosidase expression[3], while also indicating hygiene risks associated with food spoilage. Consequently, visual, rapid, and low-cost of β-galactosidase bacterial are crucial for the prevention and real-time warning of food-borne pathogen.

Monitoring enzyme activity produced by pathogens represents an effective strategy for pathogen detection[4, 5]. Bacterial enzymes exhibit high specificity towards their substrates, significantly enhancing the selectivity and precision for identifying specific strains. Various enzymes, such as alkaline phosphatase[6], tryptophanase[7], and β-galactosidase[8], have been employed as biomarkers in different sensing approaches. Although the X-Gal plate method is widely used for β-galactosidase detection, this conventional spread-plating approach requires a 12–24 h incubation, rendering it inadequate for emergency pollution incidents[9].

Traditionally, plate-counting is considered as the standard method for the evaluation of bacterial viability. In the method, the single-cell bacteria reproduce on a solid medium and finally form scattered-bacterial colonies, which are visible and numerable to human eyes. As observed, the plate count method is laborious, slow, and ill-suited for quantification analysis, owing to cumbersome plating and lengthy incubation requirements. Currently, numerous analytical techniques have already been employed for

detecting β-galactosidase, including electrochemical techniques[10, 11]luminescence assays[12, 13],and magnetic resonance technology[14]. Despite their high sensitivity and selectivity, the practical application of these methods is often limited by complex instrumentation, high costs, and cumbersome procedures[15, 16]. In contrast, colorimetric assays demonstrate significant advantages due to their simplicity, rapidity, convenience, and ability for direct visual readout.

Nanozymes have attracted significant interest[17, 18] i.e., noble metals, metal oxides, and carbon-based structures—have been engineered as potent nanozymes[19–21]. Offering cost-effectiveness, enhanced stability, and tunable activity over natural enzymes, they are widely applied in sensing, bioimaging, and environmental remediation[22–25]. Among them, Prussian blue nanoparticles (PB NPs) have attracted significant attention due to their high peroxidase-like catalytic activity, e.g., the colorimetric sensing of H_2O_2 and glucose[26]. As such, PB NPs colorimetric assays for peroxidase-based bacterial detection were explored as a visual quantitative strategy of β-galactosidase.

Herein, we present a cell-free culture, rapid, and simple colorimetric assay for β-galactosidase-positive bacteria quantitative detection in food samples. First, PB NPs catalyze the oxidation of 3,3',5,5'-tetramethylbenzidine (TMB, colorless) by H_2O_2, producing the product ox-TMB (blue), which exhibits a maximum absorption at 652 nm. Second, p-aminophenyl-β-D-galactopyranoside (PAPG), as the substrate for β-galactosidase, is hydrolyzed to the reducing agent p-aminophenol (PAP). Finally, the reducing groups of PAP react with Fe^{3+} from PB NPs, reducing it to Fe^{2+}, convert the blue signal to colorless. As seen, this reduction inhibits the catalytic activity of the PB NPs, leading to color fading and a decrease in absorbance at(abs) = 652 nm. The turnaround time between sample generation and measurement is shorter. Based on this principle, a simple, rapid and visual quantitative assay for β-galactosidase was established. Its analytical performance is compared with that of recently reported nanomaterial-based methods for *E. coli*, where the trade-off between sensitivity and accessibility that motivates the present design is made explicit.

From the perspective of biosensor classification, this work belongs to a typical enzyme-based biosensor. According to the widely accepted definition in analytical chemistry, a biosensor integrates a biological recognition element with a physicochemical transducer. Herein, the endogenous β-galactosidase from target bacteria acts as the biological recognition element, and the PB nanozyme-mediated colorimetric system serves as the optical transducer, which fully conforms to the construction principle of enzyme biosensors.

Experimental

Reagents and Materials. Potassium ferricyanide [$K_3Fe(CN)_6$], ferric chloride hexahydrate ($FeCl_3{\cdot}6H_2O$), 3,3',5,5'-tetramethylbenzidine (TMB), p-aminophenyl-β-D-galactopyranoside (PAPG), p-aminophenol (PAP), polyethylenimine (PEI, branched, Mw ~ 25,000), β-galactosidase from *E.coli* were all purchased from Shanghai Aladdin Biochemical Technology Co., Ltd. Isopropyl β-D-1-thiogalactopyranoside (IPTG) was purchased from Shanghai Macklin Biochemical Co., Ltd. o-Nitrophenyl-β-D-galactopyranoside

(ONPG) was purchased from Shanghai Yuanye Bio-Technology Co., Ltd. Phosphate buffered saline (PBS, 10 mM, pH 7.4) was purchased from Hunan Biocomma Holdings Co., Ltd. Hydrogen peroxide (H_2O_2, 30%), hydrochloric acid (HCl, 36–38%), and absolute ethanol (CH_3CH_2OH) were purchased from Xilong Scientific Co., Ltd. LB broth and nutrient agar (NA) were purchased from Beijing Luqiao Technology Co., Ltd. All reagents were of analytical grade and used as received without further purification. All solutions were prepared using ultrapure water (resistivity 18.2 MΩ·cm) obtained from a Milli-Q water purification system (Millipore, USA). All the purity of the drugs which have been mentioned is AR.

Instruments. Electronic analytical balance (BS 124S, Sartorius Instrument Systems Ltd., Beijing), electric blast drying oven (DHG-9030A, Shanghai Hong Experimental Equipment Co., Ltd.), vacuum drying oven (DZF-6020, Shanghai Qixin Scientific Instrument Co., Ltd.), ultrasonic cleaner (KQ-250B, Kunshan Ultrasonic Instrument Co., Ltd.), thermostatic heating magnetic stirrer with condenser (DF-101S, Shanghai Lichen Bangxi Instrument Technology Co., Ltd.), pH meter (PHS-3E, Shanghai Leici Instrument Co., Ltd.), constant temperature incubator shaker (TH-300, Shanghai Yiheng Scientific Instrument Co., Ltd.), autoclave, clean bench (Suzhou Purification Equipment Co., Ltd.), UV-Vis spectrophotometer (UV-5800PC, Shanghai Yuanxi Instrument Co., Ltd.), ultrasonic cell disruptor (BRANSON S-450D), field emission scanning electron microscope (SEM, Sigma 500, Zeiss, Germany), powder X-ray diffractometer (XRD, Ultima IV, Rigaku, Japan), Fourier transform infrared spectrometer (FT-IR, Nicolet iS10, Thermo Fisher Scientific, USA), X-ray photoelectron spectrometer (XPS, K-Alpha, Thermo Fisher Scientific, USA).

Synthesis of PB NPs. PEI-modified PB NPs were synthesized rapidly using a thermal method. Briefly, 10 mL of 5 mM $K_3Fe(CN)_6$ solution was added to a 50 mL round-bottom flask. A few drops of 5 M HCl solution were added to adjust the pH of the mixture to 1.12. Subsequently, 1 mL of 3% (w/v) PEI solution was added. After stirring, 10 mL of 5 mM $FeCl_3$ solution was added. The mixture was heated to 100°C and reacted for 3 h. The solution color transitioned from green to dark blue. The resulting product was centrifuged, the supernatant was discarded, and the precipitate was washed three times with deionized water. The purified PB NPs were dried in a vacuum oven at 60°C for subsequent use.

Bacterial Culture. Gram-negative bacteria [*Escherichia coli* (*E.coli*), *Pseudomonas aeruginosa* (*P. aeruginosa*), *Salmonella enterica* serovar Typhimurium (*S. Typhimurium*)] and Gram-positive bacteria [*Listeria monocytogenes* (*L. monocytogenes*), *Bacillus cereus* (*B. cereus*)] were cultured aerobically in LB broth at 37°C and 180 rpm for 12 h. The bacteria were then harvested by centrifugation at 6000 rpm for 5 min, washed three times with PBS buffer, and resuspended in PBS. The concentration was adjusted based on the optical density measured at 600 nm (OD_{600}), with OD_{600} = 1.0 corresponding to a specific concentration. Bacterial concentrations (in CFU/mL) were determined by the plate counting method: 100 μL of bacterial suspension was spread onto nutrient agar plates, incubated at 37°C, and colonies were counted. All materials contacting bacteria were sterilized at 121°C for 30 min prior to use.

Peroxidase-like Activity and Steady-State Kinetics of PB NPs. The peroxidase-like activity of PB NPs was assessed using TMB as the substrate. Typically, 60 μL of PB NPs (0.01 mg/mL), 20 μL of H_2O_2 (0.1 M), 20 μL of TMB (10 mM), and 500 μL of NaAc-HAc buffer (0.2 M, pH 4.5) were mixed. The mixture was

incubated at room temperature in the dark for 5 min. The absorption spectrum of the mixture was then recorded using a UV-Vis spectrophotometer in the range of 400–800 nm.

Steady-state kinetic assays were performed to evaluate the peroxidase-like activity of PB NPs. Reaction mixtures containing 20 μL of varying concentrations of TMB solution, 500 μL of NaAc-HAc buffer (0.2 M, pH 4.5), and 60 μL of PB NPs suspension were prepared. The absorbance of the supernatant at 652 nm was measured at 5 min intervals to investigate the effect of TMB concentration on the catalytic performance of PB NPs. The influence of TMB concentration on PB NPs catalysis in the presence of bacteria was also investigated.

Bacterial Detection Performance. Bacterial suspensions (5 mL) at varying concentrations were incubated with 50 μL of IPTG (100 mM) at 37°C and 180 rpm for 4 h to induce β-galactosidase expression. Subsequently, the bacterial cells were lysed using an ultrasonic cell disruptor, and the lysates were centrifuged to obtain bacterial supernatants containing the expressed β-galactosidase. Different concentrations of the bacterial supernatant were then mixed with 10 μL of PAPG (3.5 mM) and incubated at 37°C and 200 rpm for 1 h. Following incubation, 20 μL of H_2O_2 (0.06 M), 20 μL of TMB (8 mM), 60 μL of PB NPs (0.1 mg/mL), and 500 μL of NaAc-HAc buffer (0.2 M, pH 4.5) were added to the reaction solution. The final mixture was incubated at room temperature in the dark for 5 min. The absorbance at 652 nm was measured using a UV-Vis spectrophotometer.

Real Sample Analysis. Bottled water and milk samples were selected as representative matrices to verify the accuracy and anti-interference performance of the method. Specifically, bottled water was used as a clean water matrix with low background interference to evaluate the basic recovery performance. Milk samples were diluted 100-fold prior to analysis to prevent potential matrix interference. Spiked samples were prepared by introducing known concentrations of bacteria (*E.coli*) into the pre-treated samples.

Results and Discussion

Characterization of PB NPs. The synthesis mechanism involves electrostatic adsorption of negatively charged hexacyanoferrate(III) ions {$[Fe(CN)_6]^{3-}$} onto the positively charged PEI polymer. Subsequently, {$[Fe(CN)_6]^{3-}$} is reduced to hexacyanoferrate(II) {$[Fe(CN)_6]^{4-}$} by the imine groups on PEI. Finally, Fe^{3+} ions complex with {$[Fe(CN)_6]^{4-}$} to form PB NPs.

The UV-Vis absorption spectrum of the synthesized PB NPs (Fig. 1a) showed a characteristic broad absorption band centered at 724 nm, attributed to the metal-to-metal charge transfer (MMCT) between Fe^{2+} and Fe^{3+} ions within the Prussian blue structure. This electronic transition results in strong light absorption, producing the typical blue color, with the maximum absorption peak at 724 nm.

The chemical composition and crystallinity of the PB NPs were characterized by X-ray diffraction (XRD). As shown in Fig. 1b, the diffraction peaks centered at 2θ = 17.3°, 24.6°, 35.3°, 39.8°, 43.6°, 50.7°, 54.2°,

57.2°, 66.2°, and 69.2° correspond to the (200), (220), (400), (420), (422), (440), (600), (622), (640), and (642) crystal planes of face-centered cubic Prussian blue (JCPDS No. 73–0687). The absence of additional impurity peaks confirmed the high purity and successful synthesis of the material.

Fourier transform infrared (FT-IR) spectroscopy was used for structural analysis (Fig. 1c). The broad peak around 3450 cm^{-1} is attributed to the O-H and N-H stretching vibrations. The sharp peak at 2087 cm^{-1} is characteristic of the stretching vibration of the C ≡ N group within the Fe^{2+}-C ≡ N-Fe^{3+} bridging structure in Prussian blue. Additionally, the absorption band at 505 cm^{-1} indicates the formation of the M-CN-M' linkage (where M and M' represent metal ions). The positions of these peaks confirm the successful synthesis of Prussian blue nanoparticles.

Energy-dispersive X-ray spectroscopy (EDS) coupled with SEM was used to analyze the elemental composition. The EDS spectrum (Fig. 1d) confirmed the presence of Fe, C, and N elements in the material.

Field emission scanning electron microscopy (SEM) was employed to analyze the morphology of the PB NPs. The synthesized material consisted of relatively uniform quasi-cubic particles with smooth surfaces. The particle size ranged from approximately 50 to 100 nm, although some degree of agglomeration was observed. The cubic morphology suggests the PB NPs maintain crystalline characteristics at the microscopic scale.

The morphology and microstructure of PB NPs were directly observed by SEM and TEM. As shown in Fig. 2a, b, the as-synthesized PB NPs present a uniform quasi-cubic morphology with a particle size of approximately 50–100 nm. TEM observation (Fig. 2c, d) further confirms the cubic crystalline structure and reveals a certain degree of agglomeration among particles. Additional elemental mapping images and multi-magnification morphology images are provided in the Supporting Information (Figures S1-S3).

Figure S2 shows the elemental distribution maps. The overlay (Figure S2a) indicates the co-localization of Fe, C, and N. The individual maps for C (Figure S2b, red), N (Figure S2c, green), and Fe (Figure S2d, blue) demonstrate relatively uniform spatial distribution of these elements throughout the observed PB NP aggregates, with no significant localized enrichment.

Transmission electron microscopy (TEM) provided further insight into the morphology (Figure S3). The images confirmed the quasi-cubic shape of the particles and revealed a degree of size variation and significant agglomeration, where individual particles adhered to each other forming larger aggregates. This agglomeration could increase the effective surface area and potentially influence catalytic performance.

X-ray photoelectron spectroscopy (XPS) was used to analyze the surface elemental composition and chemical states. The survey spectrum (Fig. 3a) confirmed the presence of Fe, C, and N. The high-resolution C 1s spectrum (Fig. 3b) exhibited three deconvoluted peaks at 286.2 eV (C-N), 285.8 eV (C ≡ N), and 284.6 eV (C-C). The N 1s spectrum (Fig. 3c) showed a peak at 401.2 eV attributed to protonated

amine groups (-NH_3^+/ -NH_2^+-) from PEI, and peaks at 397.5 eV and 396.4 eV corresponding to cyanide nitrogen (-C ≡ N-) coordinated to Fe^{2+} and Fe^{3+} ions at the lattice vertices of the PB structure, respectively. The Fe 2p spectrum (Fig. 3d) revealed multiple peaks: the peak at 722.3 eV is assigned to Fe^{3+} $2p_{1/2}$, the peak at 720.3 eV to Fe^{2+} $2p_{1/2}$, the peak at 708.1 eV to Fe^{3+} $2p_{3/2}$, and the peak at 707.2 eV to Fe^{2+} $2p_{3/2}$. These assignments are consistent with the mixed valence state of iron in Prussian blue.

Peroxidase-like Activity of PB NPs. The peroxidase-like activity of the synthesized PB NPs was investigated using TMB as the substrate. As shown in Fig. 4a, solutions containing only TMB, only H_2O_2, H_2O_2 + TMB, or TMB + PB NPs exhibited negligible absorbance at 652 nm. However, in the presence of both H_2O_2 and PB NPs, a distinct blue color developed, accompanied by a strong absorption peak at 652 nm, characteristic of oxidized TMB (ox-TMB). This confirmed the peroxidase-like activity of the PB NPs. Furthermore, Fig. 4b shows that the absorbance at 652 nm increased progressively with increasing PB NPs concentration, demonstrating that the catalytic performance is concentration-dependent.

Steady-state kinetic analysis was performed to quantify the peroxidase-like activity and assess the effect of bacteria (*E.coli*) on this activity. Michaelis-Menten curves (Fig. 4c, d) and Lineweaver-Burk plots (Fig. 4e, f) were constructed based on the initial reaction velocity versus TMB concentration. Good linear fits were obtained. The Michaelis constant (K_m) values calculated from the curves in the absence and presence of *E.coli* were 9.01 mM and 7.41 mM, respectively. K_m reflects the enzyme's affinity for its substrate; a higher K_m indicates lower affinity. The higher K_m value observed in the presence of *E.coli* suggests that the bacterial components reduce the binding affinity of PB NPs for TMB.

Additionally, the calculated maximum reaction velocity (V_{max}) values were 5.68×10^{-6} M s^{-1} in the absence of *E.coli* and 4.90×10^{-6} M s^{-1} in its presence. The lower V_{max} value in the presence of bacteria indicates that, even at saturating substrate concentrations, the rate of TMB oxidation catalyzed by PB NPs is slower when bacteria are present. These results collectively demonstrate that the presence of *E.coli* reduces both the binding affinity of PB NPs for TMB and their overall catalytic activity, leading to suppressed peroxidase-like activity.

Mechanism for Detection of β-galactosidase-Positive Bacteria Using PB NPs. In this sensing system, the specific enzyme-substrate interaction between β-galactosidase and PAPG constitutes the biological recognition process, and the subsequent activity regulation of PB nanozymes and the resulting color change complete the signal transduction from biological event to readable optical signal. The detection mechanism comprises three main steps (illustrated conceptually in Fig. 4g, h): First, IPTG induces high expression of β-galactosidase in β-galactosidase-positive bacteria (e.g., *E.coli*). Next, Bacterial cells are lysed (e.g., ultrasonication) to release the intracellular β-galactosidase enzyme. Eventually, The released β-galactosidase hydrolyzes its substrate PAPG to produce PAP. The reducing groups of PAP react with Fe^{3+} ions within the PB NPs structure, reducing them to Fe^{2+}. PB NPs possess peroxidase-like activity and catalyze the oxidation of TMB by H_2O_2 to generate blue ox-TMB. However, the reduction of Fe^{3+} to

Fe^{2+} by PAP alters the Fe^{3+}/Fe^{2+} ratio and the redox potential/active sites of the PB NPs. Since Fe^{2+} sites typically lack significant peroxidase-like activity compared to the mixed-valence state, this reduction inhibits the catalytic activity of the PB NPs. Consequently, less ox-TMB is formed, leading to a decrease in blue color intensity and absorbance at 652 nm. The degree of signal suppression correlates with the concentration of β-galactosidase, and hence, the concentration of β-galactosidase-positive bacteria. This forms the basis of the colorimetric biosensor.

Using *E.coli* as a model bacterium, the mechanism was experimentally verified. Figure 4g shows that the presence of β-galactosidase alone or β-galactosidase + PAPG had a minimal effect on PB NPs activity. PAP itself caused a significant reduction in catalytic activity. Figure 4h demonstrates that while the presence of intact *E.coli* cells caused a slight decrease in absorbance, the supernatant from *E.coli* lysate incubated with PAPG (containing PAP generated by β-galactosidase hydrolysis) caused a substantial decrease in absorbance, comparable to the effect of adding PAP directly. This confirms that the inhibition is primarily due to PAP produced by the enzymatic activity of β-galactosidase released from the bacteria.

Optimization of Experimental Conditions. To achieve optimal analytical performance, key parameters of the detection system were systematically optimized. The signal used for optimization was the decrease in absorbance at 652 nm ($\Delta A = A_0 - A$) compared to the control without *E.coli* (A_0). Larger ΔA values indicate more effective signal suppression by the target bacteria. The optimized conditions were determined as follows (Figure S4): PB NPs concentration: 0.1 mg/mL;TMB concentration: 8.0 mM; H_2O_2 concentration: 0.06 M; Assay pH: 4.5 (using NaAc-HAc buffer); PAPG concentration: 3.5 mM; Incubation time for PAPG with bacterial lysate: 1 h. These optimized parameters were used for all subsequent detection experiments at 652 nm.

Specificity Test. The specificity of the method for β-galactosidase-positive bacteria was evaluated by testing against several bacterial strains at a concentration of 10^7 CFU/mL: *S. Typhimurium*, *E.coli*, *P. aeruginosa*, *L. monocytogenes*, and *B. cereus*. *P. aeruginosa* (known β-galactosidase negative) and *S. Typhimurium* (morphologically/ physiologically similar Gram-negative but β-galactosidase status varies, often negative/ weak) served as negative controls. *B. cereus* (known to produce β-galactosidase) served as a positive control alongside *E.coli*.

As shown in Fig. 4i, S. *Typhimurium*, *P. aeruginosa*, and *L. monocytogenes* caused only minor decreases in absorbance at 652 nm (small ΔA values). This slight interference might arise from the hydrolysis of PAPG by other oxidoreductases present in these bacteria. In contrast, *E.coli* and *B. cereus*, both β-galactosidase-positive, induced significantly larger decreases in absorbance (large ΔA values). The high specificity of β-galactosidase for its substrate PAPG ensures that the method exhibits significant selectivity for β-galactosidase-positive bacteria like *E.coli*. The minimal signal change caused by β-galactosidase-negative bacteria further confirms the reliability of the assay for specifically detecting target bacteria based on β-galactosidase activity.

Bacterial Detection Performance. Under the optimized conditions, the sensitivity of the detection system was evaluated using *E.coli* as the model β-galactosidase-positive bacterium. Figure 5a shows the UV-Vis absorption spectra of the reaction mixtures corresponding to increasing concentrations of *E.coli*. The absorbance intensity at 652 nm progressively decreased as the bacterial concentration increased. Figure 5b plots the signal decrease ($\Delta A = A_0 - A$) against the logarithm of *E.coli* concentration. A good linear relationship ($R^2 = 0.9984$) was observed over a wide concentration range from 8×10^1 to 8×10^7 CFU/mL. The limit of detection (LOD), estimated based on 3 times the standard deviation of the blank signal, was 8×10^1 CFU/mL. These results demonstrate that the developed colorimetric sensor possesses a broad detection range and high sensitivity for *E.coli*.

Real Sample Detection. The practical applicability of the developed colorimetric method was assessed by detecting *E.coli* spiked into bottled water and milk samples using a standard addition method. Milk samples were diluted 100-fold before spiking to minimize matrix effects. As shown in Table 1, the recoveries of *E.coli* from bottled water ranged from 100.05% to 107.43%, with relative standard deviations (RSDs) less than 4.50%. Recoveries from milk samples ranged from 97.56% to 109.41%, with RSDs also below 4.50%. These results indicate that the method provides satisfactory accuracy and precision for detecting *E.coli* in complex food and water matrices, demonstrating its good applicability for real-sample analysis. It should be clarified that the spiking concentrations in real samples were set to verify the anti-interference ability, accuracy and precision of the method in complex matrices, rather than to validate the limit of detection. The concentration gradient (2.0×10^3 – 5.0×10^5 CFU/mL) covers the common bacterial contamination level in actual polluted samples, which is a routine methodological validation design in analytical chemistry.

Meanwhile, the 100-fold dilution of milk samples is a common pretreatment strategy to eliminate matrix interference caused by proteins, fats and other macromolecular components in milk, which is widely adopted in colorimetric detection of food samples. After 100-fold dilution, the actual detection limit in raw milk is calculated to be 8000 CFU/mL. In terms of practical applicability, this detection level is suitable for rapid screening of raw milk and heavily contaminated milk samples. During the collection and transportation of raw milk, high-concentration bacterial contamination often occurs due to improper storage. The proposed method can complete quantitative detection within 5 h, which is significantly faster than the traditional plate counting method (24 h), so as to quickly screen out seriously unqualified batches and guide production control in time. According to previous literature, most nanozyme-based colorimetric methods for *E. coli* detection in milk require 10- to 100-fold dilution, and the actual detection limits in raw milk are mostly in the range of 10^3 – 10^4 CFU/mL. The sensitivity of this method is at the mainstream level of similar colorimetric methods, and has more prominent advantages in detection speed and visual readout.

Table 1
Recovery data for the detection of *E.coli* spiked into real samples (n = 3).

Sample	Added	Found	RSD	Recovery	Test by MPN (MPN/mL)
	(CFU/mL)	(CFU/mL)	(%)	(%)	
Bottled water	2.0×10^3	2.01×10^3	2.49	100.05	1.98×10^3
	1.0×10^4	1.01×10^4	3.15	101.22	1.03×10^4
	5.0×10^5	5.37×10^5	4.17	107.43	5.22×10^5
Milk	2.0×10^3	1.94×10^3	2.06	97.56	2.01×10^3
	1.0×10^4	1.03×10^4	1.32	103.50	1.17×10^4
	5.0×10^5	5.47×10^5	4.49	109.41	5.27×10^5

MPN (most probable number): multi-tube fermentation assay for low-level contaminated samples.

For practical application scenarios, this method is more suitable for water matrices with regulated *E. coli* limits and potential contamination risks, such as surface water, domestic sewage effluent, aquaculture water and food processing water. The regulatory limits of *E. coli* in these water matrices mostly fall within the linear range of the proposed method (8×10^1 – 8×10^7 CFU/mL), which can meet the demand of on-site rapid screening and graded evaluation.

Comparison with reported methods. Table S1 summarises recent nanomaterial-based methods for the determination of *E. coli* in terms of the recognition element, the reporter, the limit of detection, the working range, the assay time and the matrix. Two observations follow. First, the most sensitive formats are those that couple a high-affinity bioreceptor (antibody, aptamer or bacteriophage) to a nanoparticle reporter, and they reach 1–35 CFU/mL, i.e. one to two orders of magnitude below the present assay. Second, these gains are purchased with additional complexity: bioreceptors must be produced, purified and stored cold; sandwich formats require separation and washing steps; and SERS or electrochemical readout requires dedicated instrumentation and trained operators. The assay reported here occupies a different position in that trade-off. It uses the bacterial enzyme itself as the recognition element and a single inorganic nanozyme as the reporter, requires neither a bioreceptor nor a separation step, and is read by eye - at the cost of a limit of detection of 8×10^1 CFU/mL. The two families of methods are therefore complementary: the bioreceptor-based platforms are appropriate when trace levels must be quantified in a laboratory, whereas the present assay is appropriate when a rapid, instrument-free decision is required at the point of sampling.

Conclusions

This study successfully developed a novel colorimetric assay based on the peroxidase-like activity of Prussian blue nanoparticles (PB NPs) for the detection of β-galactosidase-positive bacteria in food samples. The method exploits the catalytic ability of PB NPs to oxidize TMB in the presence of H_2O_2, generating a blue color (ox-TMB). The key innovation lies in utilizing the β-galactosidase substrate PAPG, which is hydrolyzed by the target bacteria to produce PAP. PAP acts as a reducing agent, inhibiting the catalytic activity of PB NPs by reducing Fe^{3+} to Fe^{2+} within their structure, thereby suppressing the formation of blue ox-TMB. The degree of color suppression correlates inversely with the concentration of β-galactosidase-positive bacteria.

The developed method demonstrated excellent specificity for β-galactosidase-positive bacteria and achieved highly sensitive detection of *E.coli* over a wide linear range (8×10^1 to 8×10^7 CFU/mL), with a detection limit of 8×10^1 CFU/mL. The feasibility of the method for practical applications was successfully confirmed by detecting *E.coli* in spiked milk and bottled water samples, yielding satisfactory recovery rates and precision. Although its sensitivity (8×10^1 CFU/mL) does not match that of antibody-, aptamer- or phage-based platforms, the assay requires a single nanozyme, a single substrate and no instrument, and gives a visual answer within about 5 h. Its value therefore lies in accessibility rather than in sensitivity, which makes it attractive for hygiene screening at the point of sampling, for raw milk at an advanced stage of contamination, and as a front-end decision tool before confirmatory analysis.

Declarations

Associated content

Supporting Information. SEM images, elemental mappings, TEM images, Variation in absorbance and Comparisons with others.

Author information

Corresponding Author

Shunxing Li - College of Chemistry, Chemical Engineering & Environmental Science, Minnan Normal University, Zhangzhou, China, 363000; Fujian Province Key Laboratory of Modern Analytical Science and Separation Technology, Fujian Province University Key Laboratory of Pollution Monitoring and Control, Minnan Normal University, Zhangzhou, China, 3630003; E-mail: lishunxing@mnnu.edu.cn; Fax: 86-596-2591395.

Authors

Shangqing Li- College of Chemistry, Chemical Engineering & Environmental Science, Minnan Normal University, Zhangzhou, China, 363000.

Lingling Su- College of Chemistry, Chemical Engineering & Environmental Science, Minnan Normal University, Zhangzhou, China, 363000.

Jiayi Luo - School of Energy and Environmental Engineering, University of Science and Technology Beijing, Beijing 100083, China.

Zhaojing Huang - College of Chemistry, Chemical Engineering & Environmental Science, Minnan Normal University, Zhangzhou, China, 363000.

Fengying Zheng - College of Chemistry, Chemical Engineering & Environmental Science, Minnan Normal University, Zhangzhou, China, 363000; Fujian Province Key Laboratory of Modern Analytical Science and Separation Technology, Fujian Province University Key Laboratory of Pollution Monitoring and Control, Minnan Normal University, Zhangzhou, China, 363000.

Fengjiao Liu - College of Chemistry, Chemical Engineering & Environmental Science, Minnan Normal University, Zhangzhou, China, 363000; Fujian Province Key Laboratory of Modern Analytical Science and Separation Technology, Fujian Province University Key Laboratory of Pollution Monitoring and Control, Minnan Normal University, Zhangzhou, China, 3630003.

Luxiu Lin - College of Chemistry, Chemical Engineering & Environmental Science, Minnan Normal University, Zhangzhou, China, 363000; Fujian Province Key Laboratory of Modern Analytical Science and Separation Technology, Fujian Province University Key Laboratory of Pollution Monitoring and Control, Minnan Normal University, Zhangzhou, China, 3630003.

Jie Chen - College of Chemistry, Chemical Engineering & Environmental Science, Minnan Normal University, Zhangzhou, China, 363000; Fujian Province Key Laboratory of Modern Analytical Science and Separation Technology, Fujian Province University Key Laboratory of Pollution Monitoring and Control, Minnan Normal University, Zhangzhou, China, 363000.

Author Contributions

§**Shangqing Li,** Conceptualization, Writing - Original Draft, Methodology, Validation. §**Lingling Su,** Conceptualization, Writing - Original Draft, Methodology, Data Curation. **Jiayi Luo,** Writing - Review & Editing, Project administration. ***Shunxing Li,** Conceptualization, Resources, Supervision. **Zhaojing Huang,** Writing-review & editing, Supervision. **Fengying Zheng,** Conceptualization. **Fengjiao Liu,** Supervision. **Luxiu Lin ,** Data curation. **Jie Chen,** Investigation.

§: These authors contributed equally to this work and should be considered co-first authors.

Acknowledgements

Funding declaration

This work was supported by the Natural Science Foundation of China (22574071 and 22074058), Natural Science Foundation of Fujian Province, China (2024J01810), and the Project for the Prevention, Control, and Comprehensive Remediation of Soil Heavy Metal Pollution in Key Areas of the Huashanxi River Basin, Pinghe County, Fujian Province, China (HX2023233).

Ethics Approval declaration

No human participants or animal experiments were involved in this study. Ethical approval from an Institutional Review Board (IRB) was not required.

Competing interests

The authors declare no competing financial interest.

Additional information

Correspondence and requests for materials should be addressed to Shunxing Li.

References

1. He S, Chen Y, Wang J, et al (2024) Rapid and Sensitive Quantification of Bacterial Viability Using Ratiometric Fluorescence Sensing. Anal Chem 96:11018–11025. https://doi.org/10.1021/acs.analchem.4c01737
2. Chen Y, Jiang Y, Xue T, Cheng J (2024) Strategies for the eradication of intracellular bacterial pathogens. Biomater Sci 12:1115–1130. https://doi.org/10.1039/D3BM01498C
3. He Y, Chen J (2024) CRISPR/Cas9-Mediated Genome Editing of T4 Bacteriophage for High-Throughput Antimicrobial Susceptibility Testing. Anal Chem 96:18301–18310. https://doi.org/10.1021/acs.analchem.4c05177
4. Jiao J, Kang Q, Ma C, et al (2025) Pressure Sensor Array Based on Four DNA-Nanoenzymes with Catalase-like Activity for Portable Multiple Detection of Foodborne Pathogens. J Agric Food Chem 73:1694–1702. https://doi.org/10.1021/acs.jafc.4c09288
5. Songca SP (2022) Applications of Nanozymology in the Detection and Identification of Viral, Bacterial and Fungal Pathogens. Int J Mol Sci 23:4638. https://doi.org/10.3390/ij
6. Gwynne L, Williams GT, Yan K-C, et al (2021) TCF-ALP: a fluorescent probe for the selective detection of *Staphylococcus* bacteria and application in “smart” wound dressings. Biomater Sci 9:4433–4439. https://doi.org/10.1039/D0BM01918F
7. Liu J, Yu Z, Chen Q, Jia L (2022) L-Tryptophan assisted construction of fluorescent and colorimetric dual-channel biosensor for detection of live Escherichia coli. Microchem J 174:107085. https://doi.org/10.1016/j.microc.2021.107085
8. Miyazaki T, Park EY (2020) Crystal structure of the *Enterococcus faecalis* α-*N*-acetylgalactosaminidase, a member of the glycoside hydrolase family 31. FEBS Lett 594:2282–

2293. https://doi.org/10.1002/1873-3468.13804

9. Borah M, Yadav A, Boruah JLH, Dutta HS (2026) Paper-based single-enzyme dual-substrate assay for rapid detection and differentiation of E. coli and E. coli O157:H7. Biosens Bioelectron 304:118633. https://doi.org/10.1016/j.bios.2026.118633
10. Kwon J, Kang HY, Yang H (2021) Permeabilization-free β-galactosidase-induction-based electrochemical detection of Escherichia coli. Sens Actuators B 337:129768. https://doi.org/10.1016/j.snb.2021.129768
11. Li Q, Jin J, Lou F, et al (2018) Carbon Nanomaterials-based Electrochemical Immunoassay with β-Galactosidase as Labels for Carcinoembryonic Antigen. Electroanalysis 30:852–858. https://doi.org/10.1002/elan.201700642
12. Lozano-Torres B, Blandez JF, Sancenón F, Martínez-Máñez R (2021) Chromo-fluorogenic probes for β-galactosidase detection. Anal Bioanal Chem 413:2361–2388. https://doi.org/10.1007/s00216-020-03111-8
13. Niu Y, Wang H, Wang Y, Feng L (2021) A “turn-on” fluorescent probe for ultra-sensitive detection of β-galactosidase. Microchem J 166:106205. https://doi.org/10.1016/j.microc.2021.106205
14. Kodibagkar VD, Yu J, Liu L, et al (2006) Imaging β-galactosidase activity using ^{19}F chemical shift imaging of LacZ gene-reporter molecule 2-fluoro-4-nitrophenol-β-D-galactopyranoside. Magn Reson Imaging 24:959–962. https://doi.org/10.1016/j.mri.2006.04.003
15. Mustafa F, Liebich S, Andreescu S (2021) Nanoparticle-based amplification for sensitive detection of β-galactosidase activity in fruits. Anal Chim Acta 1186:339129. https://doi.org/10.1016/j.aca.2021.339129
16. Sharma SK, Poudel Sharma S, Leblanc RM (2021) Methods of detection of β-galactosidase enzyme in living cells. Enzyme Microb Technol 150:109885. https://doi.org/10.1016/j.enzmictec.2021.109885
17. Xiao G, Li H, Zhao Y, et al (2022) Nanoceria-Based Artificial Nanozymes: Review of Materials and Applications. ACS Appl Nano Mater 5:14147–14170. https://doi.org/10.1021/acsanm.2c03009
18. Wu J, Wang X, Wang Q, et al (2019) Nanomaterials with enzyme-like characteristics (nanozymes): next-generation artificial enzymes (II). Chem Soc Rev 48:1004–1076. https://doi.org/10.1039/C8CS00457A
19. Ma X, Xu S, Pan Y, et al (2024) Construction of SERS output-signal aptasensor using MOF/noble metal nanoparticles based nanozyme for sensitive histamine detection. Food Chem 440:138227. https://doi.org/10.1016/j.foodchem.2023.138227
20. Liu Q, Zhang A, Wang R, et al (2021) A Review on Metal- and Metal Oxide-Based Nanozymes: Properties, Mechanisms, and Applications. Nano-Micro Lett 13:154. https://doi.org/10.1007/s40820-021-00674-8
21. Zhuang Z, Yu Y, Dong S, et al (2024) Carbon-based nanozymes: design, catalytic mechanisms, and environmental applications. Anal Bioanal Chem 416:5949–5964. https://doi.org/10.1007/s00216-024-05405-7

22. Bilal M, Khaliq N, Ashraf M, et al (2023) Enzyme mimic nanomaterials as nanozymes with catalytic attributes. Colloids Surf B 221:112950. https://doi.org/10.1016/j.colsurfb.2022.112950
23. Dong Z, Liang P, Wang Y, et al (2023) The rational design of nanozymes for imaging-monitored cancer therapy. J Mater Chem B 11:5933–5952. https://doi.org/10.1039/D3TB00464C
24. Han Q, Huang D, Li S, et al (2024) Multifunctional nanozymes for disease diagnosis and therapy. Biomed J 47:100699. https://doi.org/10.1016/j.bj.2024.100699
25. Liu Q, Zhu X, Zhong L, et al (2022) Recent advances in the applications of nanozymes for the efficient detection/removal of organic pollutants: a review. Environ Sci: Nano 9:1212–1235. https://doi.org/10.1039/D2EN00027J
26. Tong L, Wu L, Zai Y, et al (2023) Paper-based colorimetric glucose sensor using Prussian blue nanoparticles as mimic peroxidase. Biosens Bioelectron 219:114787. https://doi.org/10.1016/j.bios.2022.114787

Figures

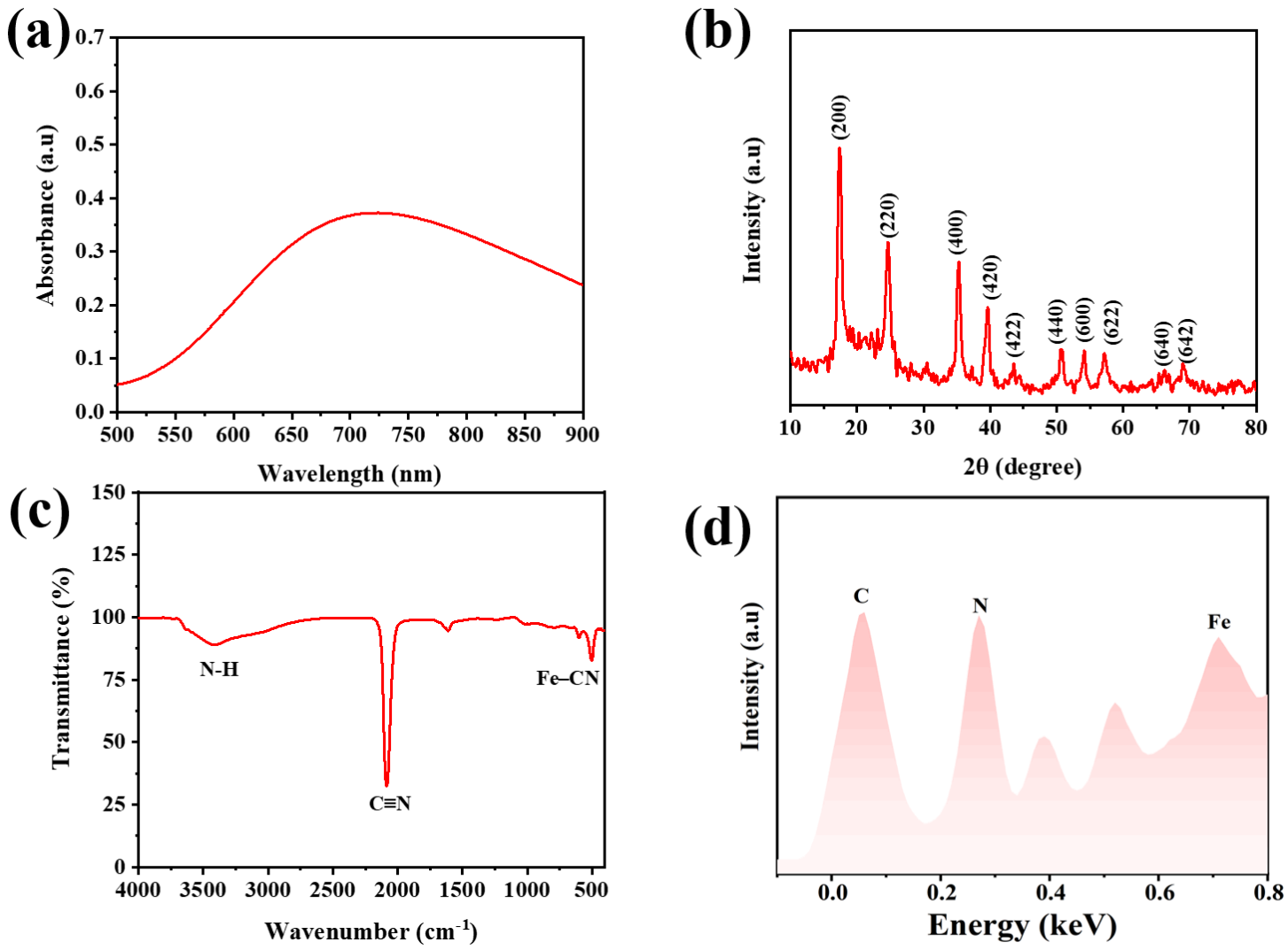

Figure 1

(a) UV-Vis absorption spectrum of PB NPs; (b) XRD pattern of PB NPs; (c) FT-IR spectrum of PB NPs. (d) EDS spectrum of PB NPs.

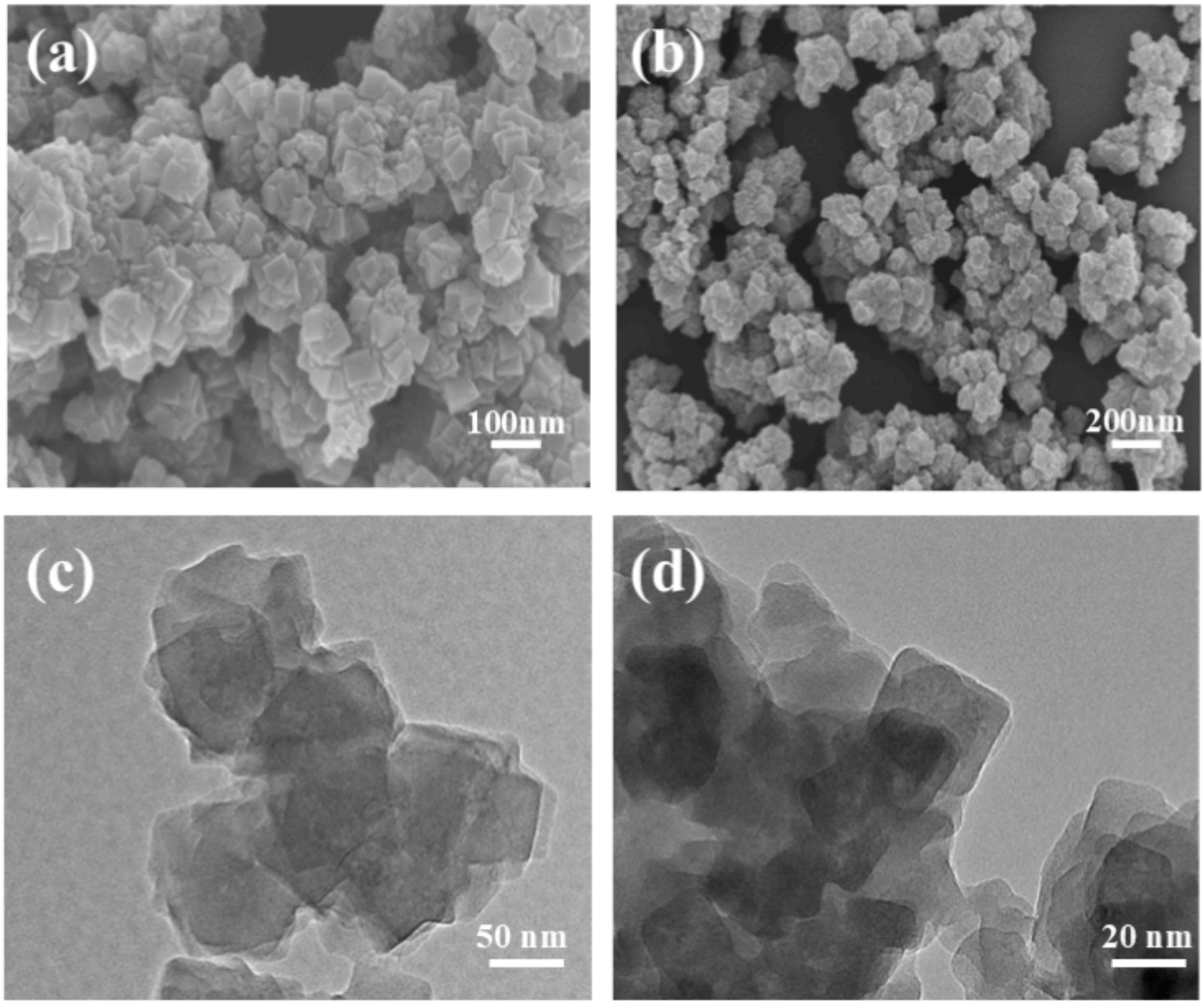

Figure 2

SEM image of PB NPs: (a) Scale bar 100 nm; (b) Scale bar 200 nm. TEM images of PB NPs: (c) Scale bar 100 nm; (d) Scale bar 200 nm.

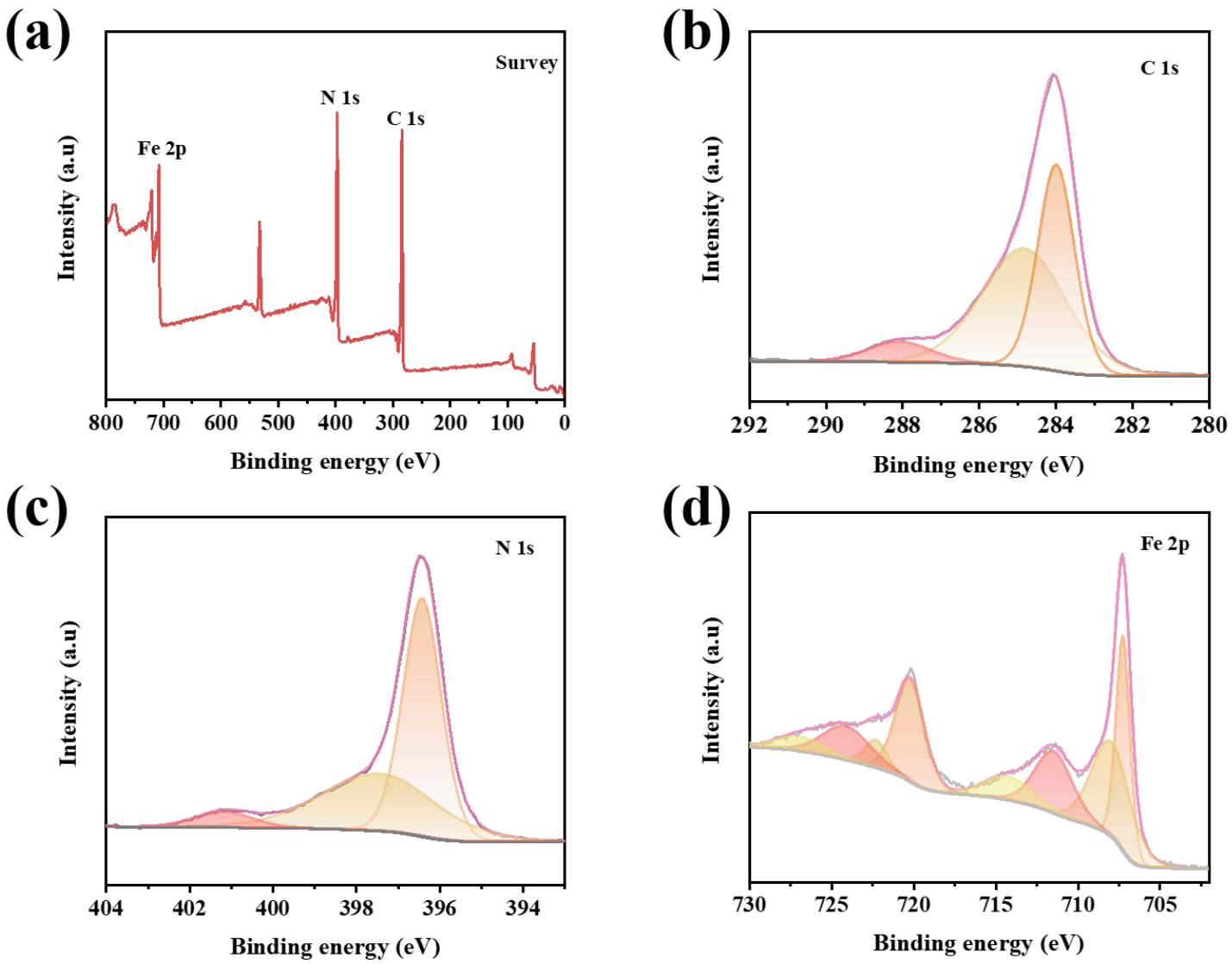

Figure 3

(a) XPS survey spectrum of PB NPs; (b) XPS survey spectrum of C;(c) XPS survey spectrum of N; (d) XPS survey spectrum of Fe.

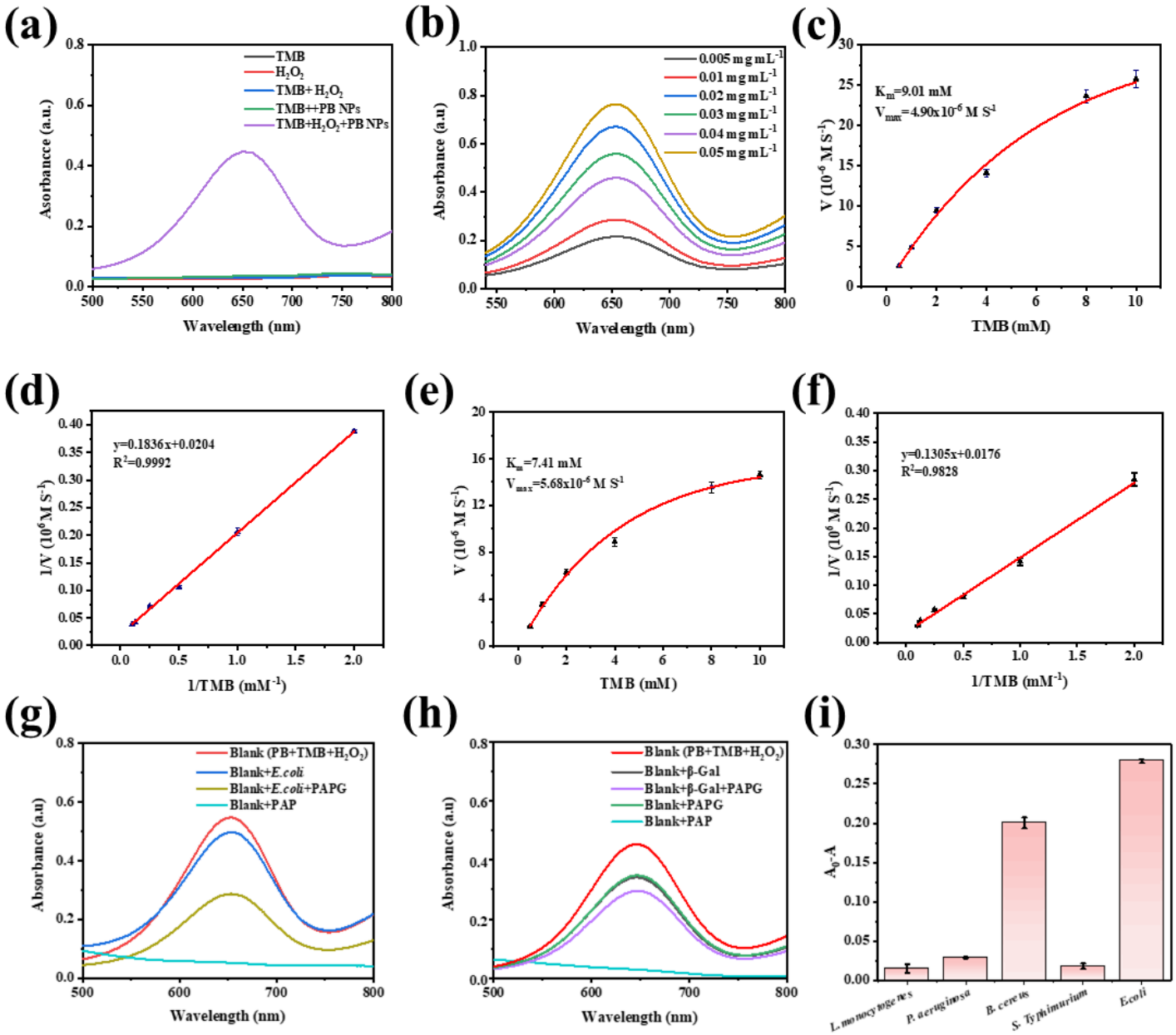

Figure 4

(a) UV-Vis absorption spectra of different reaction mixtures: TMB alone, H_2O_2 alone, TMB + H_2O_2, TMB + PB NPs, and TMB + H_2O_2 + PB NPs; (b) UV-Vis absorption spectra showing the catalytic oxidation of TMB by PB NPs at increasing concentrations (from bottom to top curve); (c) Steady-state kinetics of PB NPs catalyzing TMB oxidation: Michaelis-Menten plot in the presence of *E.coli*; (d) Michaelis-Menten plot in the absence of *E.coli*; (e) Corresponding Lineweaver-Burk plot in the presence of *E.coli*; (f) Corresponding Lineweaver-Burk plot in the absence of *E.coli*; (g) UV-Vis absorption spectra showing the effect on PB NPs catalysis: Blank (TMB + H_2O_2 +PB NPs), Blank + β-galactosidase, Blank + β-galactosidase + PAPG, Blank + PAPG, Blank + PAP; (h) UV-Vis absorption spectra showing the effect on PB NPs catalysis: Blank, Blank + *E.coli* cells, Blank + *E.coli* cells + PAPG, Blank + PAP. Significant signal suppression occurs only when PAP is present (either added directly or generated from PAPG by β-

galactosidase activity); (i) Specificity test: Signal decrease ($\Delta A = A_0 - A$) at 652 nm for different bacterial strains at 10^7 CFU/mL. *E.coli* and *B. cereus* (β-galactosidase-positive) show signifi-cantly higher ΔA compared to the other strains (β-galactosidase-negative or weak).

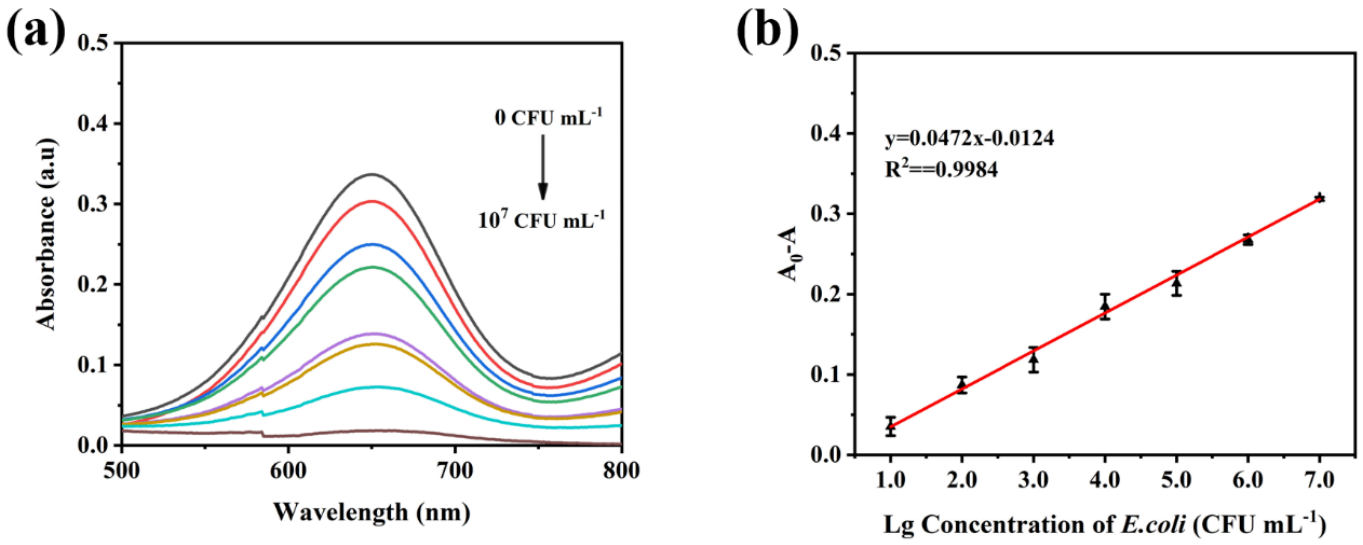

Figure 5

(a) UV-Vis absorption spectra of the detection system upon addition of increasing concentrations of *E.coli*. (b) Calibration curve: Signal decrease (ΔA) at 652 nm versus the logarithm of *E.coli* concentration (Log_{10} [CFU/mL]). Error bars represent standard deviation (n=3).

Supplementary Files

This is a list of supplementary files associated with this preprint. Click to download.

- Supplement.docx
- Graphicalabstract.png